Acta Cryst B
STRUCTURAL SCIENCE
CRYSTAL ENGINEERING
MATERIALS
ISSN 2052-5206

Structural studies of *N*-(methoxysalicylidene)-fluoroaniline, *N*-(methoxysalicylidene)-chloroaniline and *N*-(methoxysalicylidene)-bromoaniline derivatives

Helen E. Mason,[a]‡ Jane L. R. Yates,[a] Rachael J. Potts,[b] Matthias J. Gutmann,[c] Judith A. K. Howard[a] and Hazel A. Sparkes[b]*

[a]Durham University, Department of Chemistry, University Science Site, South Road, Durham, DH1 3LE, United Kingdom, [b]University of Bristol, School of Chemistry, Cantock's Close, Bristol, BS8 1TS, United Kingdom, and [c]ISIS Facility, STFC-Rutherford Appleton Laboratory, Didcot, OX11 OQX, United Kingdom. *Correspondence e-mail: hazel.sparkes@bristol.ac.uk

Received 3 June 2021
Accepted 21 September 2021

Edited by C. M. Reddy, IISER Kolkata, India

‡ Died December 2019.

Keywords: Schiff bases; thermochromism; polymorphism.

CCDC references: 2087834–2087864, 2111142–2111143

Supporting information: this article has supporting information at journals.iucr.org/b

Twenty seven *N*-(methoxysalicylidene)-haloaniline (halo = F, Cl or Br) compounds were synthesized. The crystal structures of all 27 compounds have been determined at low temperature and are reported herein, along with a variable-temperature neutron diffraction study on two of the compounds. New polymorphs were identified for two of the compounds along with a temperature-induced phase transition for one of the other compounds. Visual observations on the thermochromism of the 27 compounds are also reported. The interplanar angle between the two aromatic rings and the intermolecular interactions in the structures are examined and linked to the visual observations on the thermochromism.

1. Introduction

The relatively easy synthesis of a wide range of Schiff bases makes them versatile ligands and consequently they have found widespread use in many areas including organometallic chemistry (Kargar *et al.*, 2020), polymer synthesis (Mighani, 2020), anticancer drugs (Parveen, 2020), catalysts (Kumari *et al.*, 2019) and sensors (Sahu *et al.*, 2020). In addition, Schiff bases themselves have been found to display interesting properties with anils, Schiff bases of salicylaldehyde derivatives with aniline derivatives, having been found to exhibit both thermo- and photochromism in the solid-state (Senier & Shepheard, 1909; Cohen & Schmidt, 1962; Cohen *et al.*, 1964). Originally the thermochromism and photochromism of anils were thought to be mutually exclusive (Cohen & Schmidt, 1962; Cohen *et al.*, 1964) but this has since been found not to be the case and it is thought they all display thermochromism with some also displaying photochromism (Fujiwara *et al.*, 2004). The colour change was initially attributed to a light- or thermally-induced tautomeric equilibrium shift between colourless enol(-imine) and coloured keto(-amine) forms (Hadjoudis & Mavridis, 2004; Robert *et al.*, 2009) (see Fig. 1). In both cases the chromism involves an intramolecular proton shift from the *ortho*-hydroxy group, crucial for the mechanism to occur, to the imine nitrogen atom. Evidence for the thermochromic mechanism was first observed in *N*-(5-chlorosalicylidene)-4-hydroxyaniline with the population of the *cis*-keto form increasing with decreasing temperature, with the

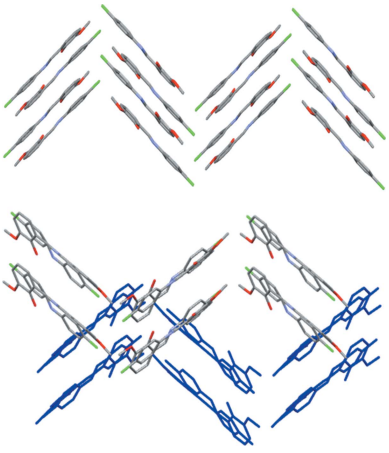

ratio of OH to NH forms changing from 31:69 at 299 K to 10:90 at 90 K (Ogawa *et al.*, 1998) and at 15 K it is believed to be solely the NH form (Ogawa *et al.*, 2000). The photochromic mechanism has been observed in single crystals of *N*-3,5-di-*tert*-butylsalicylidene-3-nitroaniline (Harada *et al.*, 1999). After 4 h irradiation at room temperature, using two-photon excitation at 730 nm, the structure of the dark-red photo product at 90 K was found to contain both the enol and *trans*-keto form at a ratio of 90:10. Irradiation at room temperature using light with $\lambda > 530$ nm caused the crystal to return to the pale yellow colour of the enol form and demonstrated the reversibility of the mechanism.

The enol–keto tautomerism is not the whole picture, Harada *et al.* identified that thermochromism in anils can only be explained by taking into account the fluorescence and not just the tautomeric equilibrium between enol and *cis*-keto forms (Harada *et al.*, 2007). The impact of the fluorescence becomes particularly significant for thermochromic compounds at lower temperatures and can in fact dominate as the cause of the thermochromic colour change. While at higher temperatures the keto–enol tautomerism is dominant for thermochromic compounds.

The synthesis of 27 *N*-(methoxysalicylidene)-haloaniline (halo = F, Cl or Br) compounds are reported. The crystal structures of all of the compounds are reported at low temperature. Ten of the structures had previously been reported at room temperature, however they are reported herein at low temperature for completeness. For two other compounds new polymorphs were identified herein while a further compound was found to undergo a temperature-induced phase transition. Visual observations were made of the thermochromic colour change upon cooling for all of the compounds. These were linked to the structural properties of the various compounds.

2. Experimental

2.1. Reagents and techniques

All reagents were used as supplied from Aldrich. Compounds were synthesized by direct condensation of the appropriate salicylaldehyde and aniline derivatives in ethanol. Salicylaldehyde (0.0025 moles) and aniline (0.0025 moles) were each dissolved in ethanol (25 ml), the resulting solutions combined and refluxed with stirring for four hours. Any precipitate was filtered off rinsed with ethanol and left to dry, the (remaining) solution was then rotary evaporated until (further) precipitate formed. Re-crystallization was carried out from ethanol and acetonitrile for all compounds. The compounds synthesized along with the reference numbers used to refer to them throughout this paper are listed in Table 1.

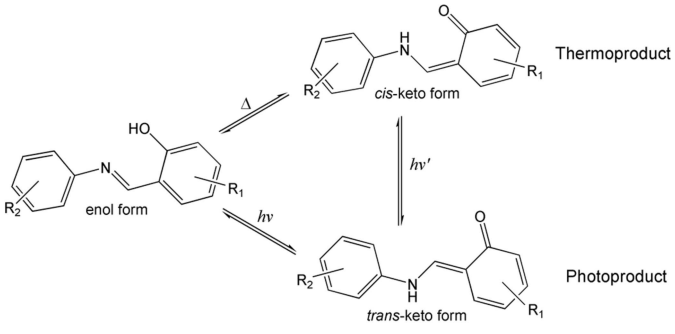

Figure 1
Illustration of the enol to keto tautomerism mechanism which affects that colour change in anils.

Table 1
Studied compounds and their reference numbers.

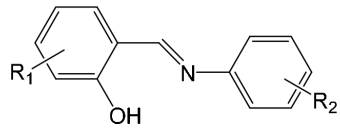

R_1 = OMe
R_2 = Br, Cl, F

Compound reference number	Substituents
1-F	R_1 = 3-OMe, R_2 = 2-F
2-F	R_1 = 4-OMe, R_2 = 2-F
3-F	R_1 = 5-OMe, R_2 = 2-F
4-F	R_1 = 3-OMe, R_2 = 3-F
5-F	R_1 = 4-OMe, R_2 = 3-F
6-F	R_1 = 5-OMe, R_2 = 3-F
7-F	R_1 = 3-OMe, R_2 = 4-F
8-F	R_1 = 4-OMe, R_2 = 4-F
9-F	R_1 = 5-OMe, R_2 = 4-F
1-Cl	R_1 = 3-OMe, R_2 = 2-Cl
2-Cl	R_1 = 4-OMe, R_2 = 2-Cl
3-Cl	R_1 = 5-OMe, R_2 = 2-Cl
4-Cl	R_1 = 3-OMe, R_2 = 3-Cl
5-Cl	R_1 = 4-OMe, R_2 = 3-Cl
6-Cl	R_1 = 5-OMe, R_2 = 3-Cl
7-Cl	R_1 = 3-OMe, R_2 = 4-Cl
8-Cl	R_1 = 4-OMe, R_2 = 4-Cl
9-Cl	R_1 = 5-OMe, R_2 = 4-Cl
1-Br	R_1 = 3-OMe, R_2 = 2-Br
2-Br	R_1 = 4-OMe, R_2 = 2-Br
3-Br	R_1 = 5-OMe, R_2 = 2-Br
4-Br	R_1 = 3-OMe, R_2 = 3-Br
5-Br	R_1 = 4-OMe, R_2 = 3-Br
6-Br	R_1 = 5-OMe, R_2 = 3-Br
7-Br	R_1 = 3-OMe, R_2 = 4-Br
8-Br	R_1 = 4-OMe, R_2 = 4-Br
9-Br	R_1 = 5-OMe, R_2 = 4-Br

2.2. Crystallographic data collection

Single crystal X-ray diffraction measurements for **1-F** to **9-F**, **7-Cl** to **9-Cl** and **1-Br** to **9-Br** were collected at 120 (2) K, **9-Br** was also collected at 220 (2) K on Bruker Smart 1K diffractometer, **1-Cl** to **3-Cl** were collected at 120 (2) K, **4-Cl** and **6-Cl** were collected at 100 (2) K and **5-Cl** was collected at 150 (2) K on a Bruker Apex II diffractometer. All datasets were collected using graphite-monochromated Mo $K\alpha$ radiation (λ = 0.71073 Å) and recorded on a CCD detector. Unit-cell parameters were also checked at 300 (2) K for all structures. Structures **1-F** to **9-F**, **7-Cl** to **9-Cl** and **1-Br** to **9-Br** were solved using direct methods in *SHELXS* (Sheldrick, 2008) and **1-Cl** to

6-Cl were solved using *Superflip* (Palatinus & Chapuis, 2007; Palatinus & van der Lee, 2008; Palatinus *et al.*, 2012). All structures were refined by full-matrix least squares on F^2 using *SHELXL* (Sheldrick, 2008, 2015) in *Olex2* (Dolomanov *et al.*, 2009). All hydrogen atoms, apart from the OH hydrogen involved in the intramolecular hydrogen bonding with the imine nitrogen atom were positioned geometrically (aromatic and C8—H8 C—H = 0.95 Å, methyl C—H = 0.98 Å) and refined using a riding model. The isotropic displacement parameter of the hydrogen atom was fixed at U_{iso}(H) = 1.2 times U_{eq} of the parent carbon atom for the aromatic hydrogen atoms and C8—H8, while U_{iso}(H) = 1.5 times U_{eq} for the parent carbon atom for the methyl hydrogens. The hydrogen atoms involved in the intramolecular hydrogen bond were located in the Fourier difference map (FDM) wherever feasible or fixed geometrically [O—H 0.84 Å, U_{iso}(H) = 1.2 times U_{eq} of the parent oxygen atom] for **6-F**, **5-Br** and **6-Br** where this was not possible. Crystal packing diagrams were created and analyzed using *Mercury* (Macrae *et al.*, 2020). The interplanar dihedral angle was calculated by measuring the angle between planes computed through the six carbon atoms of the two aromatic rings. See Tables S1–S3 in the supporting information for further details of the crystallographic data collections.

Single-crystal neutron diffraction data for **3-Cl** and **3-Br** were collected at 120 and 300 K on SXD at ISIS (Keen *et al.*, 2006) by mounting a single crystal on a closed cycle refrigerator and using 4–5 crystal settings. Data were processed using *SXD2001* (Gutmann, 2005).

2.3. Diffuse reflectance spectroscopy

Diffuse reflectance spectra were measured for **1-Br** to **9-Br**. The sample was ground to give uniform particle distribution and placed in a 40 × 10 × 2 mm quartz cuvette to ensure optical thickness. A cuvette sample holder with a white polytetrafluoroethylene (PTFE) block spacer was used to load the sample into an Oxford Instruments Cryostat. The sample was irradiated with an Ocean Optics halogen light source and an Avantes AvaSpec-2048-2 CCD detector (placed at an acute angle to minimize detection of specular reflectance) collected the reflectance spectra which were recorded using *AvaSoft* basic software. Cryostat temperature control was achieved using an Oxford Intelligent Temperature Controller, each temperature was stabilized by leaving for 10 min or waiting until a temperature variation of ±0.1 K before recording a spectrum. A white PTFE block was used to record a reference spectrum before each data set collection. The diffuse reflectance spectra are illustrated as % reflectance versus wavelength and Kubelka–Munk function, $F(R)$, versus wavelength. If S is independent of λ, then $F(R)$ versus λ is equivalent to the absorption spectrum for a diffuse reflector. To allow basic trends to be easily observed moving averages were applied to data during analysis.

3. Results and discussion

3.1. Crystal structures

The crystal structures of compounds **1-F** (Ünver *et al.*, 2002), **1-Cl** (Francis *et al.*, 2003), **2-Cl** (Koşar *et al.*, 2009), **3-Cl** (Özek *et al.*, 2008*a*), **6-Cl** (Özek *et. al.*, 2008*b*), **8-Cl** (Koşar *et al.*, 2009), **9-Cl** (Özek *et al.*, 2008*c*), **3-Br** (Özek *et al.*, 2007), **6-Br** (Özek *et al.*, 2007) and **7-Br** (Zheng *et al.*, 2005) have previously been reported. The structures obtained herein were consistent with the previously published structures. Different polymorphs to those previously published were obtained in this study for **8-F** (Albayrak *et. al.*, 2010) and **7-Cl** (Yeap *et al.*, 2003) and a phase transition upon cooling was observed for **9-Br** (Özek *et al.*, 2007). The structures reported herein will be denoted as **8-F**(2), **7-Cl**(2) and **9-Br**(LT). The structures of the remaining compounds are included here at low temperature for completeness as the published structures are at room temperature. They also demonstrate that for the majority of them no structural changes are observed upon cooling.

The 27 compounds all crystallized with one molecule in the asymmetric unit (Z' = 1) with the exception of **7-Cl**(2) which contained two unique molecules in the asymmetric unit (Z' = 2) in this study. However, the previously published polymorph of **7-Cl**(1) had one molecule in the asymmetric unit (Z' = 1) (Yeap *et al.*, 2003). The basic structure of the 27 compounds is the same containing a methoxy-substituted hydroxy-phenyl group and a halogen substituted phenyl group joined by an imine group (Fig. 2). The imine group C8═N1 bond lengths range from 1.263 (12) Å in **6-Br** to 1.299 (10) Å in **9-Br**(LT), while the hydroxyl-phenyl C2—O2 bond lengths range from 1.343 (4) Å in **8-Cl** to 1.364 (7) Å in **5-Br**. These C8═N1 and C2—O2 are consistent with the bonds being double and single bonds, respectively (Allen *et al.*, 1987), indicating that the crystal structures are all in the enol form. An intramolecular hydrogen bond creates a quasi-six-membered ring O2—H2···N1—C8—C7—C2, which shows only small deviations from planarity (maximum 0.0293 Å for **2-F**, calculated as deviations from the plane through the five non-hydrogen atoms, this value was less for the other compounds).

Examining the intermolecular interactions in the structures showed the presence of C—H···O (Gu *et al.*, 1999), and also in the case of **1-F** to **9-F** C—H···F (D'Oria & Novoa, 2008; Thalladi *et al.*, 1998) interactions in all of the structures. In addition, a small number of the structures also contained π–π

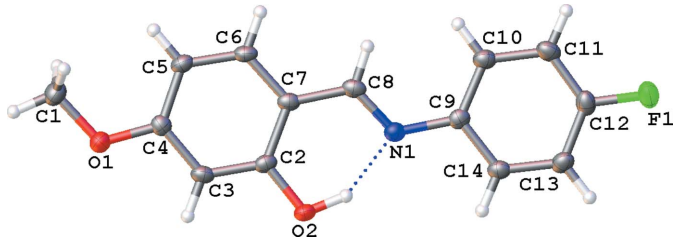

Figure 2
Structure of **8-F**(2) at 120 (2) K shown with the atomic numbering scheme. The intramolecular hydrogen bond is shown as a dotted line.

interactions (Tables S4–S8). The C—H···O interactions involve the methoxy oxygen (O1) and/or hydroxy oxygen (O2) atoms interacting mainly with aromatic C—H, although in the case of **5-F**, **8-F(2)**, **5-Cl** and **8-Br** only methyl C—H are involved (Tables S4–S6). The C—H···F interactions also mainly involve aromatic hydrogen atoms, except **9-F** which also involved a methyl hydrogen atom and **6-F** which contains either short aromatic or methyl C—H···F interactions due to the disorder in the fluorine atoms (Tables S7).

3.2. Polymorph 8-F(2)

The structure of **8-F** obtained in the current study, **8-F**(2), see Fig. 2, differs significantly from the previously published structure, denoted **8-F**(1) (Albayrak *et al.*, 2010). Both polymorphs crystallized in the monoclinic crystal system, with **8-F**(1) in the space group *Pc* while **8-F**(2) was in the space group $P2_1/c$. However, there are key differences in the molecular conformations of the two polymorphs. Firstly while both polymorphs have the methyl group of the —OMe group in approximately the same plane as the phenyl group to which it is attached, for **8-F**(1) it is on the same side as the OH group while for **8-F**(2) it is on the opposite side to the OH group. Secondly, the two phenyl rings are orientated differently with respect to each, in **8-F**(1) the dihedral angle between the two phenyl rings is 48.17 (1)° while for **8-F**(2) it is 2.07 (9)° (see Fig. 3).

The packing and intermolecular interactions for the two polymorphs are also quite different. In the case of **8-F**(1) all of the molecules are orientated in the same direction, and the structure shows C—H···F interactions between the methyl group and the fluorine atom of adjacent molecules. While in the case of **8-F**(2), C—H···F interactions exist between an aromatic H adjacent to the F on one molecule and the F on an adjacent molecule. The structure also contains π–π interactions between adjacent molecules forming a stack in approximate the *a* axis direction.

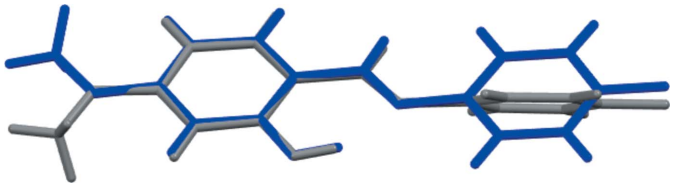

Figure 3
Overlay of a molecule of **8-F**(1) (grey) at room temperature on **8-F**(2) at 120 (2) K (blue).

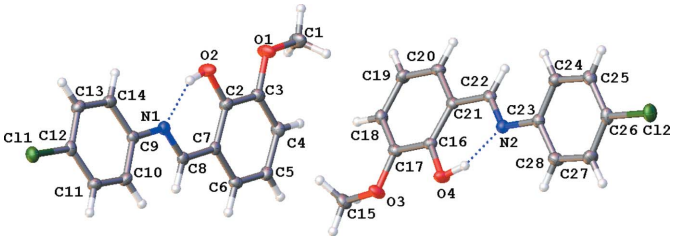

Figure 4
Structure of **7-Cl**(2) at 120 (2) K shown with the atomic numbering scheme. Intramolecular hydrogen bonding shown with dotted lines.

3.3. Polymorph 7-Cl(2)

In the case of **7-Cl**, the previously published structure [**7-Cl**(1)] (Yeap *et al.*, 2003) was obtained in the orthorhombic space group $P2_12_12_1$ with one molecule in the asymmetric unit. The dihedral angle between the two rings was ∼11.9°. The structure of **7-Cl**(2) obtained herein crystallized in the monoclinic space group $P2_1/c$ with two molecules in the asymmetric unit, see Fig. 4. The dihedral angles between the two phenyl rings were 11.75 (11)° and 16.73 (11)° for the two independent molecules, very similar to that seen for **7-Cl**(1). The structure of **7-Cl**(2), unlike **7-Cl**(1), contains Cl···Cl interactions with Cl···Cl distances of 3.3618 (7) Å and 3.3845 (7) Å. Examining the packing of the two polymorphs shows that **7-Cl**(1) forms a herringbone-type motif. While **7-Cl**(2) has a herringbone-type motif in the *ab* plane, however it is two molecules wide in the *c*-axis direction and then as a result of the *c*-glide the zigzag is the opposite direction still in the *ab* plane, see Fig. 5.

3.4. Temperature-induced phase transition 9-Br

The structure of **9-Br** (Özek *et al.*, 2007) has previously been published at room temperature in the monoclinic space group *Pc*, see Fig. 6. The structures obtained herein at 300 (2) K and 220 (2) K were consistent with the previously published structure. However, the structure was found to undergo a thermal phase transition upon cooling with no significant loss of crystallinity. At 120 (2) K the structure was found to be in

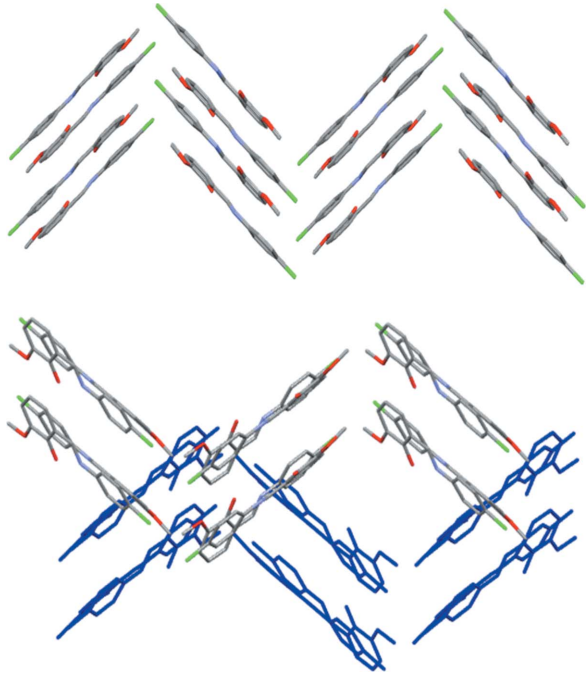

Figure 5
Packing for (top) **7-Cl**(1), (bottom) **7-Cl**(2) with front pair of molecules shown with different colours for the various elements and next pair behind in blue to show opposite zigzag direction.

the monoclinic space group *Cc*, with an approximate doubling of the *a*-axis length from 14.112 (3) Å at 300 (2) K to 27.874 (5) Å at 120 (2) K and a reduction in the β angle from 98.326 (4)° at 300 (2) K to 95.091 (4)° at 120 (2) K. The orientation of the molecule did not change significantly as a result of the phase transition, see Fig. 7, and the packing in both cases was almost identical.

3.5. Thermochromic observations

The anils are known to display thermochromism. Here all of the 3- or 5-methoxysalicylaldimine derivatives were found to be orange/red at room temperature and showed a reversible colour change to yellow when dipped in liquid nitrogen (∼77 K). The 4-methoxysalicylaldimine derivatives appear yellow at room temperature and show little or no colour change to the naked eye with decreasing temperature (see Fig. 8 for a representative example). The colour change for the strongly thermochromic compounds can also be followed clearly by eye as a function of temperature, see Fig. 9.

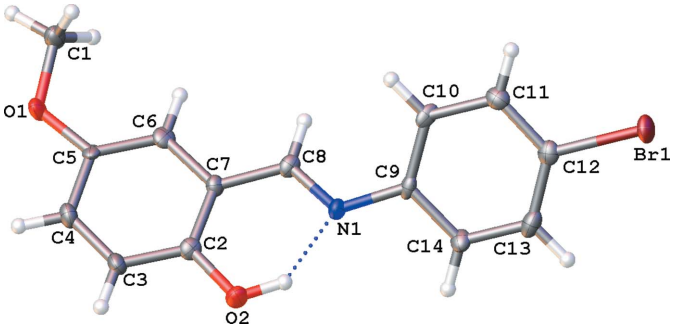

Figure 6
Structure of **9-Br** at 120 (2) K shown with the atomic numbering scheme. The intramolecular hydrogen bond is shown with as a dotted line.

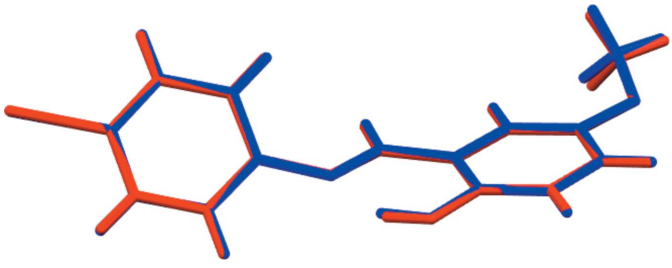

Figure 7
Overlay of a molecule of **9-Br** at 300 (2) K (red) on **9-Br** at 120 (2) K (blue).

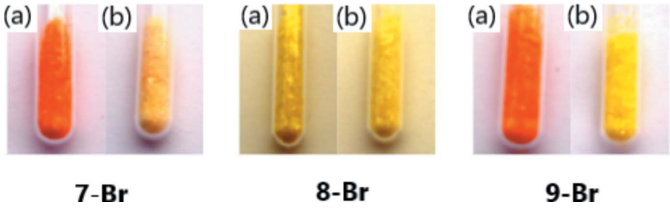

Figure 8
Microcrystalline powders of (left) **7-Br**, (middle) **8-Br** and (right) **9-Br** at (*a*) room temperature and (*b*) after dipping in liquid nitrogen.

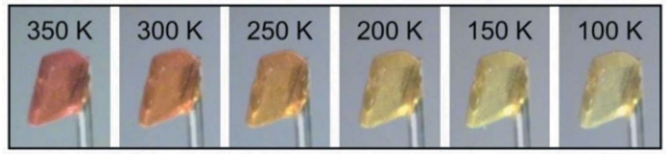

Figure 9
Illustration of the colour change upon cooling for **4-F**.

The thermochromic colour change was initially believed to be due solely to an enol to *cis*-keto tautomerism with the enol form being colourless and the keto form being coloured (Hadjoudis & Mavridis, 2004; Robert *et al.*, 2009). However, it has also been found that temperature-induced fluorescence also plays a significant role in the colour change observed, particularly upon cooling (Harada *et al.*, 2007). Diffuse reflectance spectra were collected for **1-Br** to **9-Br** and are available in Figs. S1–S9. No account was taken of the potential effect of fluorescence, however the spectra are presented to support the visually observed trends. In the reflectance spectra for the more strongly thermochromic complexes (**1**, **3**, **4**, **6**, **7** and **9**) the reflectance decreases rapidly below ∼580 nm as the temperature is reduced, which is consistent with a lightening in colour. While for the weakly thermochromic compounds (**2**, **5** and **8**) much smaller decreases in reflectance were observed upon cooling below ∼490 nm. To look for evidence of proton transfer in two of the crystals showing significant colour changes, **3-Cl** and **3-Br**, variable-temperature neutron diffraction was carried out. However, no evidence of the proton shifting was identified and the O—H proton was located at essentially the same position at both 300 (2) and 120 (2) K for both structures. It is possible that the level of the *cis*-keto form was too small to be detected crystallographically.

3.6. Structural analysis

A packing similarity tree diagram for the structures, calculated using CSD Materials in *Mercury* (Macrae *et al.*,

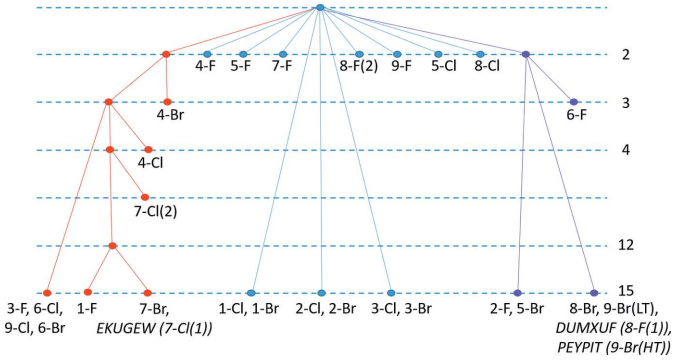

Figure 10
Packing similarity diagram calculated using *CSD Materials* in *Mercury* (Macrae *et al.*, 2020) and allowing for structural variations. Both polymorphs of **8-F** and **7-Cl** are included along with the 300 K (HT) and 120 K (LT) structures of **9-Br**.

Table 2
Dihedral angles (φ) (°) between the two phenyl rings for all of the compounds.

Both polymorphs of **7-Cl** and **8-F** are included. Note **7-Cl**(2) has $Z' = 2$.

Compound prefix	Halogen position	OMe position	F	Cl	Br
1	2	3	6.19 (11)	7.20 (10)	6.9 (2)
2	2	4	56.75 (7)	24.15 (5)	23.70 (8)
3	2	5	5.66 (7)	11.13 (7)	13.86 (13)
4	3	3	30.60 (8)	0.60 (11)	24.09 (11)
5	3	4	2.40 (11)	28.38 (5)	42.72 (12)
6	3	5	29.52 (4)	5.64 (15)	5.4 (7)
7	4	3	10.48 (5)	**7-Cl**(1)† 11.9° **7-Cl**(2) 11.75 (11) 16.73 (11)	10.9 (4)
8	4	4	**8-F**(1)‡ 48.17 (1) **8-F**(2) 2.07 (9)	16.3 (2)	48.67 (7)
9	4	5	20.60 (4)	7.71 (9)	38.42 (16)

† Yeap *et al.* (2003). ‡ Albayrak *et al.* (2010).

2020) and allowing for structural variations, highlights both links between structures with similar packing and the wide range of packing observed, Fig. 10. The point at which structures meet at a node highlights the number of molecules in a cluster around the central molecule that are similar so for example **1-F** and **7-Br** have 12 molecules in common while **1-Cl** and **1-Br** are essentially isostructural with fifteen molecules in common. For completeness the location of the three published structures which differ from the structures determined in this study have been included on the diagram. Unsurprisingly for **9-Br** which undergoes a space group change upon cooling (*Pc* to *Cc*) the packing in the room temperature structure (Özek *et al.*, 2007) has a very high similarity to the 120 (2) K structure. In general, it is worth noting that the structures showing high similarity in their packing with ≥ 12 molecules in common, in the cluster around the central molecule that are similar, tend to be pairs or groups that are either moderately/strongly thermochromic or weakly thermochromic. The main exception to this rule is that the weakly thermochromic **8-F** and **8-Br** have very similar structures to **9-Br** which by eye show a larger colour change.

The dihedral angles between the two phenyl rings are given in Table 2 and show wide variations from 2.07 (9)° in **8-F**(2) to 56.74 (7)° in **2-F**. In some Schiff bases a link between the dihedral angle and chromic behaviour has been proposed (Hadjoudis & Mavridis, 2004; Robert *et al.*, 2009), compounds with $\varphi < 25°$ are expected to be strongly thermochromic due to the higher basicity of the imine nitrogen and as φ increases the degree of thermochromism is expected to reduce. In the compounds studied here there is some variation from this expected trend with three of the strongly thermochromic compounds **4-F**, **6-F** and **9-Br** having large φ values of 30.60 (8)°, 29.53 (4)° and 38.42 (16)°, respectively, while three of the weakly thermochromic compounds **5-F**, **8-F**(2) and **8-Cl** have very small or small φ values of 2.40 (11)°, 2.07 (9)° and 16.33 (20)°, respectively. No significant correlation between the halogen substituent position and the thermochromic behaviour was identified in this study.

4. Conclusions

The structures of 27 *N*-(methoxysalicylidene)-haloaniline (halo = F, Cl or Br) are reported at 150 (2), 120 (2) or 100 (2) K. Ten of these structures had previously been reported at room temperature and the structures herein were the same. While in the case of **8-F** and **7-Cl** new polymorphs are reported which show significant differences in their packing compared to the previously reported polymorphs. In addition, a phase transition was identified for **9-Br**, which occurs somewhere between 200 (2) and 120 (2) K. No phase transitions were identified between 300 (2) and 120 (2) K for any of the other compounds.

The 4-methoxysalicyl derivatives are yellow at room temperature and display very little colour change by eye when dipped in liquid nitrogen, ~77 K, whereas the 3- or 5-methoxysalicyl compounds are orange–red at room temperature and show a dramatic colour change with decreasing temperature down to yellow at liquid nitrogen temperatures. The colour change has previously been associated with the occurrence of a temperature-induced enol to *cis*-keto tautomerism with temperature-induced fluorescence also having a significant impact. Herein neutron diffraction studies on **3-Cl** and **3-Br** showed no evidence of proton shifting, so it is possible that the level of the *cis*-keto form was too small to be detected crystallographically but also no investigation was made into the effect of fluorescence on the or the colour change in the complexes.

While both the nature of the packing and the compounds' interplanar angle are believed to affect the thermo- and photochromic properties of the anils, the type and position of substituents can also be important. The position of the strongly electron donating methoxy group on the salicyl moiety appears to have a stronger influence on the colour and thermochromic properties of the anils than the location of the weakly electron withdrawing halogen on the aniline moiety. The 3- and 5-methoxy compounds visually showed significant colour changes upon cooling, while the 4-methoxy compounds showed relatively small colour changes. While the majority of the 3- and 5-methoxy compounds had dihedral angles φ of < 25° there were several exceptions to the rule.

Acknowledgements

The authors are grateful to Professor Andrew Beeby, Durham University, for help with discussions on the chromism. HEM is grateful to the EPSRC and Durham University for funding and Professor Jonathan Steed, Durham University for useful discussions.

References

Albayrak, C., Özek, A., Koşar, B., Odabaşoğlu, M. & Büyükgüngör, O. (2010). *Acta Cryst.* E**66**, o315.
Allen, F. H., Kennard, O., Watson, D. G., Brammer, L., Orpen, A. G. & Taylor, R. (1987). *J. Chem. Soc. Perkin Trans.* 2, pp. S1–S19.
Cohen, M. D. & Schmidt, G. M. J. (1962). *J. Phys. Chem.* **66**, 2442–2446.

Cohen, M. D., Schmidt, G. M. J. & Flavian, S. (1964). *J. Chem. Soc.* pp. 2041–2051.
Dolomanov, O. V., Bourhis, L. J., Gildea, R. J., Howard, J. A. K. & Puschmann, H. (2009). *J. Appl. Cryst.* **42**, 339–341.
D'Oria, E. & Novoa, J. J. (2008). *CrystEngComm*, **10**, 423–436.
Francis, S., Muthiah, P. T., Venkatachalam, G. & Ramesh, R. (2003). *Acta Cryst.* E**59**, o1045–o1047.
Fujiwara, T., Harada, J. & Ogawa, K. (2004). *J. Phys. Chem. B*, **108**, 4035–4038.
Gu, Y. L., Kar, T. & Scheiner, S. (1999). *J. Am. Chem. Soc.* **121**, 9411–9422.
Gutmann, M. J. (2005). *SXD2001*. ISIS Facility, Rutherford Appleton Laboratory, Oxfordshire, England.
Hadjoudis, E. & Mavridis, I. M. (2004). *Chem. Soc. Rev*. **33**, 579–588.
Harada, J., Fujiwara, T. & Ogawa, K. (2007). *J. Am. Chem. Soc.* **129**, 16216–16221.
Harada, J., Uekusa, H. & Ohashi, Y. (1999). *J. Am. Chem. Soc.* **121**, 5809–5810.
Kargar, H., Torabi, V., Akbari, A., Behjatmanesh-Ardakani, R., Sahraei, A. & Tahir, M. N. (2020). *J. Mol. Struct.* **1205**, 127642.
Keen, D. A., Gutmann, M. J. & Wilson, C. C. (2006). *J. Appl. Cryst.* **39**, 714–722.
Koşar, B., Albayrak, C., Odabaşoğlu, M. & Büyükgüngör, O. (2009). *Acta Cryst.* C**65**, o517–o520.
Kumari, S., Das, B. & Ray, S. (2019). *Dalton Trans.* **48**, 15942–15954.
Macrae, C. F., Sovago, I., Cottrell, S. J., Galek, P. T. A., McCabe, P., Pidcock, E., Platings, M., Shields, G. P., Stevens, J. S., Towler, M. & Wood, P. A. (2020). *J. Appl. Cryst.* **53**, 226–235.
Mighani, H. (2020). *J. Polym. Res.* **27**, 168.
Ogawa, K., Harada, J., Tamura, I. & Noda, Y. (2000). *Chem. Lett.* **29**, 528–529.
Ogawa, K., Kasahara, Y., Ohtani, Y. & Harada, J. (1998). *J. Am. Chem. Soc.* **120**, 7107–7108.
Özek, A., Albayrak, C., Odabaşoğlu, M. & Büyükgüngör, O. (2007). *Acta Cryst.* C**63**, o177–o180.
Özek, A., Albayrak, Ç., Odabaşoğlu, M. & Büyükgüngör, O. (2008*b*). *J. Chem. Crystallogr.* **39**, 353–357.
Özek, A., Büyükgüngör, O., Albayrak, C. & Odabaşoğlu, M. (2008*a*). *Acta Cryst.* E**64**, o1579–o1580.
Özek, A., Büyükgüngör, O., Albayrak, C. & Odabaşoğlu, M. (2008*c*). *Acta Cryst.* E**64**, o1613–o1614.
Palatinus, L. & Chapuis, G. (2007). *J. Appl. Cryst.* **40**, 786–790.
Palatinus, L., Prathapa, S. J. & van Smaalen, S. (2012). *J. Appl. Cryst.* **45**, 575–580.
Palatinus, L. & van der Lee, A. (2008). *J. Appl. Cryst.* **41**, 975–984.
Parveen, S. (2020). *Appl. Organomet. Chem.* **2020**, e5687.
Robert, F., Naik, A. D., Tinant, B., Robiette, R. & Garcia, Y. (2009). *Chem. Eur. J.* **15**, 4327–4342.
Sahu, M., Manna, A. K., Rout, K., Mondal, J. & Patra, G. K. (2020). *Inorg. Chim. Acta*, **508**, 119633.
Senier, A. & Shepheard, F. G. (1909). *J. Chem. Soc. Trans.* **95**, 1943–1955.
Sheldrick, G. M. (2008). *Acta Cryst.* A**64**, 112–122.
Sheldrick, G. M. (2015). *Acta Cryst.* C**71**, 3–8.
Thalladi, V. R., Weiss, H. C., Bläser, D., Boese, R., Nangia, A. & Desiraju, G. R. (1998). *J. Am. Chem. Soc.* **120**, 8702–8710.
Ünver, H., Kendi, E., Güven, K. & Durlu, T. N. (2002). *Z. Naturforsch.* **57**, 685–690.
Yeap, G.-Y., Ha, S.-T., Ishizawa, N., Suda, K., Boey, P.-L. & Kamil Mahmood, W. A. (2003). *J. Mol. Struct.* **658**, 87–99.
Zheng, C.-S., Yang, N., Li, M. & Jing, Z.-L. (2005). *Acta Cryst.* E**61**, o3613–o3614.